

Detuning-Dependent Mollow Triplet of a Coherently-Driven Single Quantum Dot

Ata Ulhaq,^{1,2} Stefanie Weiler,¹ Sven Marcus Ulrich,¹ Michael Jetter,¹
and Peter Michler¹

¹ *Institut für Halbleiteroptik und Funktionelle Grenzflächen, Allmandring 3, 70569 Stuttgart, Germany*

² *Department of Physics School of Science and Engineering, Lahore University of Management Sciences Sector U, DHA, Lahore 54792 Pakistan*
s.weiler@ihfg.uni-stuttgart.de

Chiranjeeb Roy and Stephen Hughes

Department of Physics, Engineering Physics and Astronomy, Queens's University, Kingston, Ontario, Canada K7L 3N6
shughes@physics.queensu.ca

Abstract: We present both experimental and theoretical investigations of a laser-driven quantum dot (QD) in the dressed-state regime of resonance fluorescence. We explore the role of phonon scattering and pure dephasing on the detuning-dependence of the Mollow triplet and show that the triplet sidebands may spectrally broaden or narrow with increasing detuning. Based on a polaron master equation approach which includes electron-phonon interaction nonperturbatively, we derive a fully analytical expression for the spectrum. With respect to detuning dependence, we identify a crossover between the regimes of spectral sideband narrowing or broadening. A comparison of the theoretical predictions to detailed experimental studies on the laser detuning-dependence of Mollow triplet resonance emission from single In(Ga)As QDs reveals excellent agreement.

© 2018 Optical Society of America

OCIS codes: (270.0270) Quantum optics; (300.6320) Spectroscopy, high-resolution; (300.6470) Spectroscopy, semiconductors

References and links

1. A. Muller, E. B. Flagg, P. Bianucci, X. Y. Wang, D. G. Deppe, W. Ma, J. Zhang, G. J. Salamo, M. Xiao, and C. K. Shih, "Resonance Fluorescence from a Coherently Driven Semiconductor Quantum Dot in a Cavity," *Phys. Rev. Lett.* **99**, 187402, (2007).
2. E. B. Flagg, A. Muller, J. W. Robertson, S. Founta, D. G. Deppe, M. Xiao, W. Ma, G. J. Salamo, and C. K. Shih, "Resonantly driven coherent oscillations in a solid-state quantum emitter," *Nat. Phys.* **5** 203-207 (2009).
3. A. Nick Vamivakas, Yong Zhao, Chao-Yang Lu, and Mete Atatüre, "Spin-resolved quantum-dot resonance fluorescence," *Nat. Physics* **5**, 198-202 (2009).
4. A. Kiraz, M. Atatüre, and A. Imamoglu, "Quantum-dot single-photon sources: Prospects for applications in linear optics quantum-information processing," *Phys. Rev. A* **69**, 032305 (2004).
5. S. Ates, S. M. Ulrich, S. Reitzenstein, A. Löffler, A. Forchel, and P. Michler, "Post-Selected Indistinguishable Photons from the Resonance Fluorescence of a Single Quantum Dot in a Microcavity," *Phys. Rev. Lett.* **103**, 167402 (2009).
6. C. Matthiesen, A. N. Vamivakas, and Atatüre, "Subnatural Linewidth Single Photons from a Quantum Dot," *Phys. Rev. Lett.* **108**, 093602 (2012).
7. H S. Nguyen, C Voisin, P. Roussignol, C. Diedrichs, and G Cassabois, "Ultra-coherent single photon source," *App. Phys. Lett.* **99**, 261904 (2011).

8. A. Ulhaq, S. Weiler, S. M. Ulrich, R. Roßbach, M. Jetter, and P. Michler, “Cascaded single-photon emission from resonantly excited quantum dots,” *Nat. Photonics* **6**, 238 (2012).
9. C. Roy, and S. Hughes, “Influence of Electron-Acoustic-Phonon Scattering on Intensity Power Broadening in a Coherently Driven Quantum-Dot-Cavity System,” *Phys. Rev. X* **1**, 021009 (2011).
10. C. Förstner, C. Weber, J. Danckwerts, and A. Knorr, “Phonon-Assisted Damping of Rabi Oscillations in Semiconductor Quantum Dots,” *Phys. Rev. Lett.* **91**, 127401 (2003).
11. P. Machnikowski, and L. Jacak, “Resonant nature of phonon-induced damping of Rabi oscillations in quantum dots,” *Phys. Rev. B* **69**, 193302 (2004).
12. K. J. Ahn, J. Förstner, and A. Knorr, “Resonance fluorescence of semiconductor quantum dots: Signatures of the electron-phonon interaction,” *Phys. Rev. B* **71**, 153309 (2005).
13. A. Vagov, M. D. Croitoru, V. M. Axt, T. Kuhn, and F. M. Peeters, “Nonmonotonous Field Dependence of Damping and Reappearance of Rabi Oscillations in Quantum Dots,” *Phys. Rev. Lett.* **98**, 227403 (2007).
14. A. Nazir, “Photon statistics from a resonantly driven quantum dot,” *Phys. Rev. B* **78**, 153309, (2008).
15. C. Roy, and S. Hughes, “Phonon-Dressed Mollow Triplet in the Regime of Cavity Quantum Electrodynamics: Excitation-Induced Dephasing and Nonperturbative Cavity Feeding Effects,” *Phys. Rev. Lett.* **106**, 247403 (2011).
16. C. Roy, H. Kim, E. Waks, and S. Hughes, “Anomalous phonon-mediated damping of a driven quantum dot embedded in a high-Q microcavity,” *Photon Nanostruct: Fundam. Appl.* **10** 359 (2012).
17. A. J. Ramsay, A. V. Gopal, E. M. Gauger, A. Nazir, B. W. Lovett, A. M. Fox, and M. S. Skolnick, “Damping of Exciton Rabi Rotations by Acoustic Phonons in Optically Excited InGaAs/GaAs Quantum Dots,” *Phys. Rev. Lett.* **104**, 017402 (2010).
18. S. M. Ulrich, S. Ates, S. Reitzenstein, A. Löffler, A. Forchel, and P. Michler, “Dephasing of Mollow Triplet Sideband Emission of a Resonantly Driven Quantum Dot in a Microcavity,” *Phys. Rev. Lett.* **106**, 247402, (2011).
19. B. R. Mollow, “Power Spectrum of Light Scattered by Two-Level Systems,” *Phys. Rev.* **188**, 169-175 (1969).
20. I. Wilson-Rae and A. Imamoglu, “Quantum dot cavity-QED in the presence of strong electron-phonon interactions,” *Phys. Rev. B* **65**, 235311 (2002).
21. D. P. S. McCutcheon and A. Nazir, “Quantum dot Rabi rotations beyond the weak exciton-phonon coupling regime,” *New J. Phys.* **12**, 113042 (2010).
22. G. D. Mahan, *Many-Particle Physics*, Plenum, New York, 1990.
23. L. Besombes, K. Kheng, L. Marsal, and H. Mariette, “Acoustic phonon broadening mechanism in single quantum dot emission,” *Phys. Rev. B* **63**, 155307 (2001).
24. P. Borri, W. Langbein, S. Schneider, U. Woggon, R. L. Sellin, D. Ouyang, and D. Bimberg, “Ultralong Dephasing Time in InGaAs Quantum Dots,” *Phys. Rev. Lett.* **87**, 157401 (2001).
25. E. A. Muljarov and R. Zimmermann, “Dephasing in Quantum Dots: Quadratic Coupling to Acoustic Phonons,” *Phys. Rev. Lett.* **93**, 237401 (2004).
26. M. Bayer and A. Forchel, “Temperature dependence of the exciton homogeneous linewidth in $\text{In}_{0.60}\text{Ga}_{0.40}\text{As}/\text{GaAs}$ self-assembled quantum dots,” *Phys. Rev. B* **65**, 041308 (2002).
27. G. Ortner, D. R. Yakovlev, M. Bayer, S. Rudin, T. L. Reinecke, S. Fafard, Z. Wasilewski, and A. Forchel, “Temperature dependence of the zero-phonon linewidth in InAsGaAs quantum dots,” *Phys. Rev. B* **70**, 201301(R) (2004).
28. B. Krummheuer, V. M. Axt, and T. Kuhn, “Theory of pure dephasing and the resulting absorption line shape in semiconductor quantum dots,” *Phys. Rev. B* **65**, 195313 (2002).
29. J. Förstner, C. Weber, J. Danckwerts, and A. Knorr, “Phonon-Assisted Damping of Rabi Oscillations in Semiconductor Quantum Dots,” *Phys. Rev. Lett.* **91**, 127401 (2003).
30. C. Roy and S. Hughes, “Polaron master equation theory of the quantum-dot Mollow triplet in a semiconductor cavity-QED system,” *Phys Rev B* **85**, 115309 (2012).
31. In order to derive the phonon scattering rates, we use parameters for InAs/GaAs QDs, which are $\omega_b = 1 \text{ meV}$ and $\alpha_p/(2\pi)^2 = 0.15 \text{ ps}^2$, where ω_b is the high frequency cutoff proportional to the inverse of the typical electronic localization length in the QD and α_p is a material parameter (extracted from our experiments) that accounts for the difference between the deformation potential constants between electrons and holes.
32. G. S. Agarwal and R. R. Puri, “Cooperative behavior of atoms irradiated by broadband squeezed light,” *Phys. Rev. A* **41**, 3782 (1990)
33. Anders Moelbjerg, Per Kaer, Michael Lorke, and Jesper Mørk “Resonance Fluorescence from Semiconductor Quantum Dots: Beyond the Mollow Triplet,” *Phys. Rev. Lett.* **108**, 017401 (2012).
34. D. P. S. McCutcheon, N. S. Dattani, E. M. Gauger, B. W. Lovett, and A. Nazir, “A General Approach to Quantum Dynamics Using a Variational Master Equation: Application to Phonon-Damped Rabi Rotations in Quantum Dots,” *Phys. Rev. B* **84**, 081305(R) (2011).
35. e.g., see M. Glässl, A. Vagov, S. Lüker, D. E. Reiter, M. D. Croitoru, P. Machnikowski, V. M. Axt, and T. Kuhn, “Long-time dynamics and stationary nonequilibrium of an optically driven strongly confined quantum dot coupled to phonons,” *Phys. Rev. B* **84**, 195311 (2011).
36. e.g., see H. J. Carmichael, *Statistical Methods in Quantum Optics 1: Master Equations and Fokker-Planck Equations*, Springer (2003).

37. M. Bissiri, G. Baldassarri Höger von Högersthal, A. S. Bhatti, M. Capizzi, A. Frova, P. Figeri, and S. Franchi, “Optical evidence of polaron interaction in InAs/GaAs quantum dots,” *Phys. Rev. B* **62**, 46428 (2000).
 38. S. Hughes, P. Yao, F. Milde, A. Knorr, D. Dalacu, M. Mnaymneh, V. Sazonova, P. J. Poole, G. C. Aers, J. Lapointe, R. Cheriton, and R. L. Williams, “Influence of electron-acoustic phonon scattering on off-resonant cavity feeding within a strongly coupled quantum-dot cavity system,” *Phys. Rev. B* **83**, 165313 (2011).
 39. Dara P. S. McCutcheon, and Ahsan Nazir, “Emission properties of a driven artificial atom: increased coherent scattering and off-resonant sideband narrowing,” arXiv:1208.4620v1
-

1. Introduction

Resonant excitation of single QDs has recently gained a lot of interest [1–3], in part because this type of coherent excitation is promising for the generation of single photons with excellent coherence properties [4]. The techniques developed for effective laser stray light suppression have enabled the collection of resonance fluorescence from a single QD with high signal-to-noise ratio. Resonance fluorescence (RF) emission below saturation of the quantum emitter has revealed close-to-Fourier limited single photons with record-high emission coherence and two-photon interference visibility [5]. Recent experiments have even been able to beat the Fourier limit for single-photon emission coherence in the Heitler regime, e.g., with excitation strengths well below those to saturate the quantum emitter [6, 7]. Another major achievement with respect to RF is the demonstration of single- and cascaded photon emission between the Mollow sidebands above saturation of the QD [8].

Recent investigations of single QD RF have revealed distinct differences of their emission coherence properties [9] which need to be theoretically treated beyond a simple two-level description usually used for atoms.

One of the main consequences of the solid-state character of these quantum emitters is the consideration of specific dephasing channels primary caused by carrier-phonon scattering. Dephasing of a resonantly driven QD system has been theoretically studied in detail with respect to electron-phonon interaction on the dynamics of an optically driven system [10–12]. These studies anticipated excitation-induced dephasing (EID) for moderate Rabi frequencies. However, non-monotonic behavior was predicted for Rabi frequencies larger than a cut-off frequency defined by the material parameters and the QD size [13, 14]. Non-monotonic behavior is also predicted for cavity structures with suitable cavity coupling [15, 16]. Experimental evidence of EID effects has recently been observed as oscillation damping in pulsed photocurrent measurements on a resonantly driven QD [17]. This damping was found to have a clear quadratic dependence on the effective Rabi frequency Ω . The effect of EID has also been observed under strictly resonant continuous wave excitation of a QD in a microcavity in terms of Mollow-triplet sideband broadening [18]. These experiments reveal good agreement with a theoretical description based on a polaron master equation approach to multi-phonon and multi-photon effects in a cavity-QED system [15]. In the work of Ulrich *et al.* [18], the phenomenon of spectral Mollow sideband *narrowing* in dependence of laser-excitation detuning from the bare emitter resonance had to be left open for further in-depth theoretical analysis.

Motivated by these findings and with the aim of fundamental interpretation, the focus of the current work lies on a detailed study of the detuning-dependent dressed state emission of a single QD without cavity coupling. Our theory is based on a polaron master equation approach from which we develop a fully analytical description of the emission spectrum. We are able to distinguish between different regimes of spectral broadening or narrowing of the Mollow sidebands, under strong influence by pure dephasing and phonon-induced scattering. The comparison of detuning-dependent resonance fluorescence data reveals very good agreement with the theoretical model.

2. Sample Structure and Experimental Procedure

The planar sample employed for the measurements in this work is grown by metal-organic vapor epitaxy (MOVPE). The self-assembled In(Ga)As QDs are embedded in a GaAs λ -cavity, sandwiched between 29 (4) periods of $\lambda/4$ -thick AlAs/GaAs layers as the bottom (top) distributed Bragg reflectors (DBRs). For our experimental investigations, the sample is kept in a Helium flow cryostat providing high temperature stability $T = 5 \pm 0.5$ K. Suppression of parasitic laser stray-light is achieved by use of an orthogonal geometry between QD excitation and emission detection. In addition, polarization suppression and spatial filtering via a pinhole is applied in the detection path. Resonant (tunable) QD excitation is achieved by a narrow-band (≈ 500 kHz) continuous-wave (cw) Ti:Sapphire ring laser. For high-resolution spectroscopy (HRPL) of micro-photoluminescence (μ -PL) we employ a scanning Fabry-Pérot interferometer with $\Delta E_{\text{res}}^{\text{HRPL}} < 1 \mu\text{eV}$ as described earlier [5, 8, 18]).

3. Experimental Results: Detuning-Dependent Resonance Fluorescence

In our experiments we apply pump powers well above the saturation of the quantum emitters. In this high-field regime, the excitation-induced Rabi rotation of the two-level emitter system becomes much faster than the spontaneous decay rate γ . The incoherent spectrum of the resulting dressed state is the characteristic Mollow triplet [19]. Under strictly resonant excitation, i.e. for a laser detuning $\Delta = \omega_L - \omega_x = 0$ from the QD exciton resonance (see Fig. 1(a), green center trace) and the spectrum is composed of the central *Rayleigh line* “R” at the bare emitter energy ω_0 and two symmetric satellite peaks, i.e. the *Three Photon Line* “T” and the *Fluorescence Line* “F” at $\omega_0 \pm \Omega_r$, respectively. Ω_r denotes the effective Rabi frequency including renormalization effects from the phonon bath as discussed in the theory section below.

Laser detuning (Δ)-dependent Mollow triplet spectra taken at a constant excitation strength of $P_0 = 500 \mu$ ($\Omega_r \propto (P_0)^{1/2} = \text{const.}$) are depicted in Fig. 1(a). According to theory (see, e.g. Ref. [3]), the laser-detuning between the driving field and the bare emitter resonance ω_0 modifies the dressed emission. Besides the center transition at $\omega_0 + \Delta$ the two sideband fre-

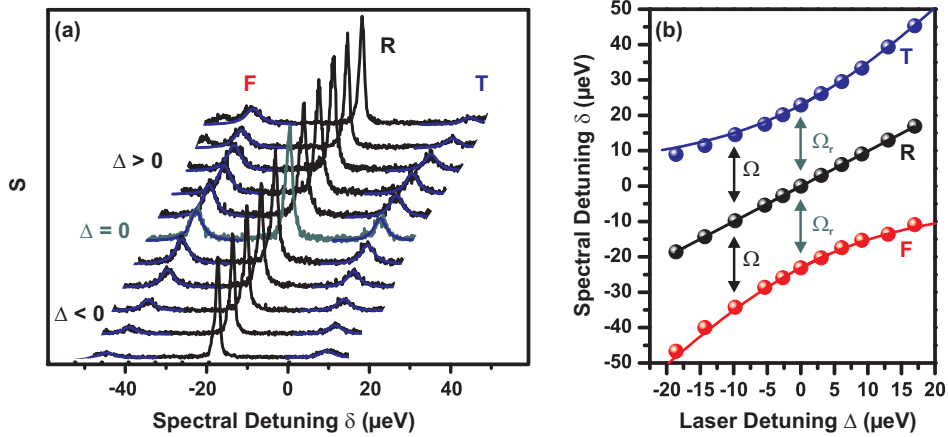


Fig. 1: (a) HRPL of the QD resonance fluorescence under systematic variation of the laser-excitation detuning $\Delta = \omega_L - \omega_x$, taken at a fixed power of $P_0 = 500 \mu\text{W}$. δ denotes the spectral emission detuning from the bare emitter resonance. Green center trace: Mollow triplet under strictly resonant excitation $\Delta = 0$. (b) Spectral evolution of the Mollow sidebands with laser-detuning Δ , extracted from (a).

quencies become $\omega_0 + \Delta \pm \Omega$, where $\Omega = \sqrt{\Omega_r^2 + \Delta^2}$ denotes the generalized Rabi frequency at a given excitation strength. The extracted spectral positions for the red- and blue-shifted Mollow sidebands and the central Rayleigh line are depicted in Fig. 1(b) with a corresponding fit to the data. In addition, observations on the detuning-dependent Mollow triplet series depicted in Fig. 1(a) reveal distinct broadening of the Mollow sidebands with increasing Δ , accompanied by a change in the relative sideband intensities. In order to explain these observations, we will develop a theoretical description in terms of a polaron master equation formalism and derive an analytical expression for the incoherent spectrum. The main theoretical findings used to interpret our experimental observations are described in the following section.

4. Theory

4.1. Hamiltonian, Polaron Master Equations and Phonon Scattering Rates

We model the QD as a effective two-level system interacting with a coherent pump field and an acoustic phonon reservoir. In a frame rotating with respect to the laser pump frequency ω_L , the model Hamiltonian (excluding QD zero-phonon line decay) is

$$H = -\hbar\Delta\sigma^+\sigma^- + \hbar\eta_x(\sigma^+ + \sigma^-) + \sigma^+\sigma^- \sum_q \hbar\lambda_q(b_q + b_q^\dagger) + \sum_q \hbar\omega_q b_q^\dagger b_q, \quad (1)$$

where $b_q(b_q^\dagger)$ are the annihilation and creation operators of the phonon reservoir, $\sigma^{+/-}$ (and $\sigma^z = \sigma^+\sigma^- - \sigma^-\sigma^+$) are the Pauli operators of the exciton. η_x is the exciton pump rate, and λ_q (assumed real) is the coupling strength of the electron-phonon interaction. In order to include electron-phonon scattering nonperturbatively, we transform the above Hamiltonian to the polaron frame. Consequently, we derive a polaron master equation (ME) [9, 15, 20, 21] which is particularly well suited for studying quantum optical phenomena such as resonance fluorescence spectra. In the following we will closely follow (and extend where necessary) the theoretical formalisms described in Refs. [9, 15], except we can neglect cavity terms.

Defining $P = \sigma^+\sigma^- \sum_q \frac{\lambda_q}{\omega_q}(b_q^\dagger - b_q)$, then the polaron transformed Hamiltonian, $H' \rightarrow e^P H e^{-P}$ [22], consists of a system part, reservoir part, and an interaction part, respectively:

$$H'_S = \hbar(-\Delta - \Delta_P)\sigma^+\sigma^- + \langle B \rangle X_g, \quad H'_R = \sum_q \hbar\omega_q b_q^\dagger b_q, \quad H'_I = X_g \zeta_g + X_u \zeta_u, \quad (2)$$

with the coherent displacement operators B_\pm defined as $B_\pm = \exp[\pm \sum_q \frac{\lambda_q}{\omega_q}(b_q - b_q^\dagger)]$, and $\zeta_g = \frac{1}{2}(B_+ + B_- - 2\langle B \rangle)$ and $\zeta_u = \frac{1}{2i}(B_+ - B_-)$. The polaron shift is $\Delta_P = \int_0^\infty d\omega \frac{J(\omega)}{\omega}$, where $J(\omega) = \alpha_p \omega^3 \exp(-\frac{\omega^2}{2\omega_b^2})$ denotes the characteristic phonon spectral function that describes the LA-phonon interaction resulting from deformation potential coupling. The thermally-averaged bath displacement operator is defined through [22] $\langle B \rangle = \exp\left[-\frac{1}{2} \int_0^\infty d\omega \frac{J(\omega)}{\omega^2} \coth(\beta\hbar\omega/2)\right]$, with $\langle B \rangle = \langle B_+ \rangle = \langle B_- \rangle$, at a bath temperature $T = 1/k_b\beta$. For convenience, we will assume that the polaron shift is implicitly included in our definition of ω_x below. The operators X_g and X_u are defined through $X_g = \hbar\eta_x(\sigma^- + \sigma^+)$ and $X_u = i\hbar\eta_x(\sigma^+ - \sigma^-)$.

We next present the time-local (or time-convolutionless) ME for the reduced density operator $\rho(t)$ of the QD-bath system in the second-order Born approximation of the system-reservoir coupling. In the interaction picture, we consider the exciton-photon-phonon coupling H'_I in the Born approximation and trace over the phonon degrees of freedom. The *full polaron ME* takes

the following form [9, 15, 20, 21]:

$$\begin{aligned} \frac{\partial \rho}{\partial t} = & \frac{1}{i\hbar} [H'_S, \rho(t)] + \frac{\gamma}{2} \mathcal{L}[\sigma^-] + \frac{\gamma'}{2} \mathcal{L}[\sigma_{11}] \\ & - \frac{1}{\hbar^2} \int_0^t d\tau \sum_{m=g,u} \left(G_m(\tau) \left[X_m, e^{-iH'_S \tau/\hbar} X_m e^{iH'_S \tau/\hbar} \rho(t) \right] + \text{H.c.} \right), \end{aligned} \quad (3)$$

where $\sigma_{11} = \sigma^+ \sigma^-$ and the time-dependent function $G_\alpha(t) \equiv \langle \zeta_\alpha(t) \zeta_\alpha(0) \rangle$ is derived as follows: $G_g(t) = \langle B \rangle^2 (\cosh[\phi(t)] - 1)$ and $G_u(t) = \langle B \rangle^2 \sinh[\phi(t)]$ [20, 22], with the phonon correlation function $\phi(t) = \int_0^\infty d\omega \frac{J(\omega)}{\omega^2} [\coth(\beta\hbar\omega/2) \cos(\omega t) - i \sin(\omega t)]$. The Lindblad operators $\mathcal{L}[O] = 2O\rho O^\dagger - O^\dagger O\rho - \rho O^\dagger O$ describe dissipation through zero-phonon line (ZPL) radiative decay (γ) and ZPL pure dephasing (γ'), where the latter process is known to increase as a function of temperature [23–27]. Without the coherent pump term and the residual ZPL broadenings, this ME formally recovers the independent boson model [22, 28, 29].

For continuous wave (cw) excitation, the integration appearing in Eq. (3) can have the upper time limit $t \rightarrow \infty$, resulting in a Markovian ME where the scattering rates are computed as a function of H'_S [30]. Such an approach is valid since the acoustic phonon lifetimes are very fast, i.e. on a few ps timescale. As was shown earlier [9], for the pump strengths we consider, one can neglect the pump-dependence of H'_S appearing in the exponential phase terms above (which we will further justify below) to derive an *effective phonon ME* as

$$\begin{aligned} \frac{\partial \rho}{\partial t} = & \frac{1}{i\hbar} [H'_S, \rho(t)] + \frac{\gamma}{2} \mathcal{L}[\sigma^-] + \frac{\gamma'}{2} \mathcal{L}[\sigma_{11}] + \frac{\Gamma_{\text{ph}}^{\sigma^+}}{2} \mathcal{L}[\sigma^+] + \frac{\Gamma_{\text{ph}}^{\sigma^-}}{2} \mathcal{L}[\sigma^-] \\ & - \Gamma_{\text{ph}}^{\text{cd}} (\sigma^+ \rho \sigma^+ + \sigma^- \rho \sigma^-) . \end{aligned} \quad (4)$$

Here the pump-driven incoherent scattering processes, mediated by the phonon bath, are obtained from

$$\Gamma_{\text{ph}}^{\sigma^+/\sigma^-} = \frac{\Omega_r^2}{2} \text{Re} \left[\int_0^\infty d\tau e^{\pm i\Delta\tau} (e^{\phi(\tau)} - 1) \right], \quad (5)$$

and

$$\Gamma_{\text{ph}}^{\text{cd}} = \frac{\Omega_r^2}{2} \text{Re} \left[\int_0^\infty d\tau \cos(\Delta\tau) (1 - e^{-\phi(\tau)}) \right] . \quad (6)$$

The classical Rabi frequency of the exciton pump, including renormalization effects from the phonon bath, is given by $\Omega_r = 2\eta_x \langle B \rangle$ (in contrast to the bare Rabi frequency $\Omega_0 = 2\eta_x$). The scattering term $\Gamma_{\text{ph}}^{\text{cd}}$ is a cross-dephasing rate that only affects the off-diagonal components of the resulting optical Bloch equations. Similar terms appear when a system is driven by a broadband squeezed light reservoir [32] and are sometimes referred to as ‘‘anomalous correlations’’. As might be expected, the excitation-dependent rates depend upon the phonon correlation function, the coherent pump rate, and the laser-exciton detuning. The $\Gamma_{\text{ph}}^{\sigma^-}$ process corresponds to an *enhanced radiative decay*, while the $\Gamma_{\text{ph}}^{\sigma^+}$ process represents an *incoherent excitation* process [15]. We stress that these mechanisms are quite different to simple pure dephasing models, which are frequently used to describe weak (i.e., perturbative) electron-phonon scattering [33]. Note that Ω_r can be significantly smaller than Ω_0 , even at low temperatures. For example, using InAs QD parameters that closely represent our experimental samples [31] and a phonon bath temperature T 6K, then $\langle B \rangle \approx 0.75$, and this value decreases (increases) with increasing (decreasing) temperature.

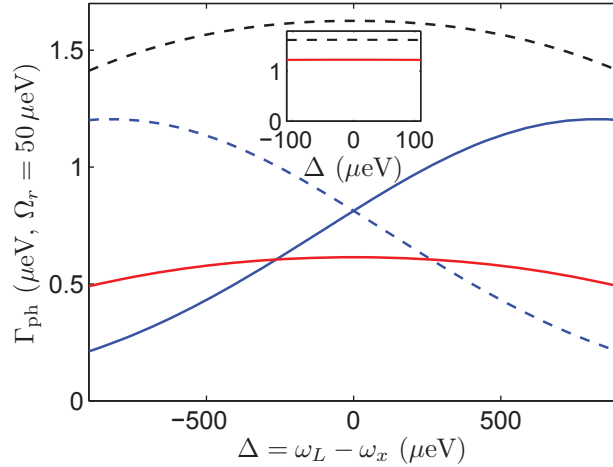


Fig. 2: Phonon-mediated scattering rates $\Gamma_{\text{ph}}^{\sigma+/-}$ (blue solid and dashed lines, respectively), together with their average sum (black dashed line) and $\Gamma_{\text{ph}}^{\text{cd}}$ (red solid line) for a phonon bath temperature $T = 6$ K. Only for large detunings $\Delta = \omega_L - \omega_x \geq 0.5$ meV these rates change appreciably. The overall magnitude of the phonon scattering rates is proportional to Ω_r^2 . Here we assume $\Omega_r = 50$ μeV . As is shown in the inset figure, the sum of rates $\Gamma_{\text{ph}}^{\sigma+} + \Gamma_{\text{ph}}^{\sigma-}$ as well as $\Gamma_{\text{ph}}^{\text{cd}}$ are constant within laser-exciton detunings over hundreds of μeV .

For a pump field strength of $\Omega_r = 50$ μeV , example phonon scattering rates are shown in Fig. 2. Within the zoomed region of laser detunings $|\Delta| < 100$ μeV the relevant rates can be assumed to be constant. Therefore, these values will be treated as constant in the following to compute the analytical Mollow triplets.

4.2. Mollow Triplet Simulations: Full Polaron versus Effective Phonon ME

To get better insight into the underlying physics, it is desirable to derive an analytical form for the Mollow triplet spectrum, which we derive from the effective phonon ME. Thus we will first investigate how good the approximation is to replace the phonon scattering terms in the *full* polaron ME [Eq. (3)] by the ones appearing in the *effective* phonon ME [Eq. (4)]. In Fig. 3, a direct comparison between the numerically calculated Mollow triplet based on the full polaron and the effective phonon ME is shown, revealing excellent agreement even for large detunings $\Delta = 30$ μeV and high field strengths of $\Omega_0 = 50$ μeV . The main reason that one can neglect the pump-dependence of the phase terms in Eq. (3) is that—for the pump values we consider—one ps timescale, phonon correlation times are much faster than the inverse Rabi oscillation.

We highlight that a cw Rabi field of $\Omega_r = 50$ μeV is already close to the highest achievable experiments to date, and thus for our purposes can be considered the high-field regime. However, we note that the polaron approach, although nonperturbative, can break down if extremely high field strengths are used such that Ω_r becomes comparable to (or greater than) the phonon cut-off frequency. In this case, other approaches exist such as a variational master equation approach [34] and path integral techniques [35]. Since our maximum Rabi field strengths are much less than ω_b , as shown by McCutcheon *et al.* [34], the polaron ME should be rigorously valid for the field strengths that we model.

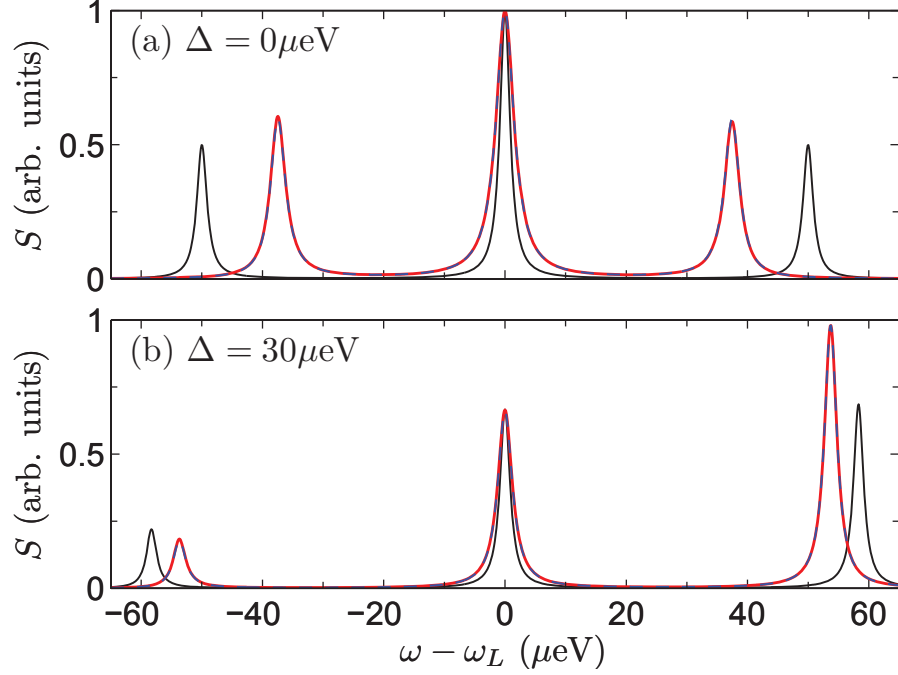


Fig. 3: Numerically calculated Mollow triplet with $\Omega_0 = 50 \mu\text{eV}$ ($\gamma = \gamma' = 1 \mu\text{eV}$, phonon bath temperature $T = 6 \text{ K}$), for (a) $\Delta = 0 \mu\text{eV}$ and (b) $\Delta = 30 \mu\text{eV}$, plotted for the case of no phonon scattering (black solid line), and with phonon scattering using the full polaron ME (red solid line) and the effective ME (blue dashed line). The latter two are found to give almost identical spectra, which justifies the accuracy of the simpler effective ME. Additionally, the effect of renormalization of the Rabi frequency can be seen in the different Mollow triplet center-to-sideband splittings for the case of no phonon scattering (black line) in comparison to the red spectrum.

4.3. Optical Bloch Equations and Analytical Fluorescence Spectrum

One of our main theoretical goals is to derive a useful analytical expression that will allow one to fit the experimental Mollow triplets over a wide range of parameters, including the laser-exciton detuning. From the effective phonon ME [Eq. (4)] and $\langle \dot{O} \rangle = \text{tr}\{\dot{\rho}O\}$ [36], we obtain the following optical Bloch equations:

$$\frac{d\langle \sigma^- \rangle}{dt} = -(\gamma_{\text{pol}} + i\Delta)\langle \sigma^- \rangle - \gamma_{\text{cd}}\langle \sigma^+ \rangle - i\frac{\Omega_r}{2}\langle \sigma^z \rangle, \quad (7a)$$

$$\frac{d\langle \sigma^+ \rangle}{dt} = -(\gamma_{\text{pol}} - i\Delta)\langle \sigma^+ \rangle - \gamma_{\text{cd}}\langle \sigma^- \rangle + i\frac{\Omega_r}{2}\langle \sigma^z \rangle, \quad (7b)$$

$$\frac{d\langle \sigma^z \rangle}{dt} = -i\Omega_r\langle \sigma^- \rangle + i\Omega_r\langle \sigma^+ \rangle - \gamma_{\text{pop}}\langle \sigma^z \rangle - \gamma'_{\text{pop}}, \quad (7c)$$

where we define the polarization decay $\gamma_{\text{pol}} = \frac{1}{2}(\Gamma_{\text{ph}}^{\sigma^+} + \Gamma_{\text{ph}}^{\sigma^-} + \gamma + \gamma')$ and the population decay $\gamma_{\text{pop}} = (\Gamma_{\text{ph}}^{\sigma^+} + \Gamma_{\text{ph}}^{\sigma^-} + \gamma)$, as well as $\gamma'_{\text{pop}} = \gamma_{\text{pop}} - 2\Gamma_{\text{ph}}^{\sigma^+}$. For notational convenience, we have also defined $\gamma_{\text{cd}} \equiv \Gamma_{\text{ph}}^{\text{cd}}$. The incoherent spectrum can be computed from an integration of the

appropriate two-time correlation function [36]:

$$S(\mathbf{r}, \omega) \equiv F(\mathbf{r})S(\omega) = F(\mathbf{r}) \frac{1}{\pi} \lim_{t \rightarrow \infty} \text{Re} \left\{ \int_0^\infty d\tau \langle \delta\sigma^+(t) \delta\sigma^-(t+\tau) \rangle e^{i(\omega - \omega_L)\tau} \right\}, \quad (8)$$

where $\langle \delta O \rangle = \langle O \rangle - O$ and $F(\mathbf{r})$ is a geometrical factor. The coherent spectrum can be derived in a similar way. By exploiting the quantum regression theorem and equation set (7a)-(7c), it is possible to derive the spectrum analytically, e.g., using Laplace transform techniques. We first define the steady-state expectation values $f(0) \equiv \langle \delta\sigma^+ \delta\sigma^- \rangle_{ss}$, $g(0) \equiv \langle \delta\sigma^+ \delta\sigma^+ \rangle_{ss}$, and $h(0) \equiv \langle \delta\sigma^+ \delta\sigma^z \rangle_{ss}$, and keep the explicit laser-exciton detuning dependence in the solution. Defining $\delta\omega = \omega - \omega_L$, we can obtain the spectrum from

$$S(\omega) = \frac{1}{\pi} \text{Re}[f(\delta\omega, \Delta)], \quad (9)$$

where

$$f(\delta\omega, \Delta) = \frac{-f(0) \left[i\delta\omega - \gamma_{\text{pop}} + \frac{\Omega_r^2/2}{i\delta\omega - (\gamma_{\text{pol}} - i\Delta)} \right] + \frac{i\Omega_r}{2} \left[-h(0) + \frac{ig(0)\Omega_r}{i\delta\omega - (\gamma_{\text{pol}} - i\Delta)} \right]}{[i\delta\omega - (\gamma_{\text{pol}} + i\Delta)](i\delta\omega - \gamma_{\text{pop}}) + \frac{\Omega_r^2 [i\delta\omega - \gamma_{\text{pol}} - \gamma_{\text{cd}}/2]}{i\delta\omega - (\gamma_{\text{pol}} - i\Delta)}}. \quad (10)$$

The steady-state inversion and polarization components are

$$\begin{aligned} \langle \sigma^s \rangle_{ss} &= -\frac{\gamma'_{\text{pop}}}{\gamma_{\text{pop}} + \frac{\Omega_r^2 (\gamma_{\text{pol}} + \gamma_{\text{cd}})/2}{(\gamma_{\text{pol}}^2 + \Delta^2 - \gamma_{\text{cd}}^2)}}, \\ \langle \sigma^+ \rangle_{ss} &= \frac{\frac{-i\Omega_r}{2} [(\gamma_{\text{pol}} + i\Delta) + \gamma_{\text{cd}}]}{(\gamma_{\text{pol}}^2 + \Delta^2 - \gamma_{\text{cd}}^2)} = (\langle \sigma^- \rangle_{ss})^*, \end{aligned} \quad (11)$$

from which we can obtain the following steady-state values for f , g , and h :

$$f(0) = \frac{1}{2} (1 + \langle \sigma^z \rangle_{ss} - \langle \sigma^+ \rangle_{ss} \langle \sigma^- \rangle_{ss}), \quad (12a)$$

$$g(0) = -\langle \sigma^+ \rangle_{ss}^2, \quad (12b)$$

$$h(0) = -\langle \sigma^+ \rangle_{ss} (1 + \langle \sigma^z \rangle_{ss}). \quad (12c)$$

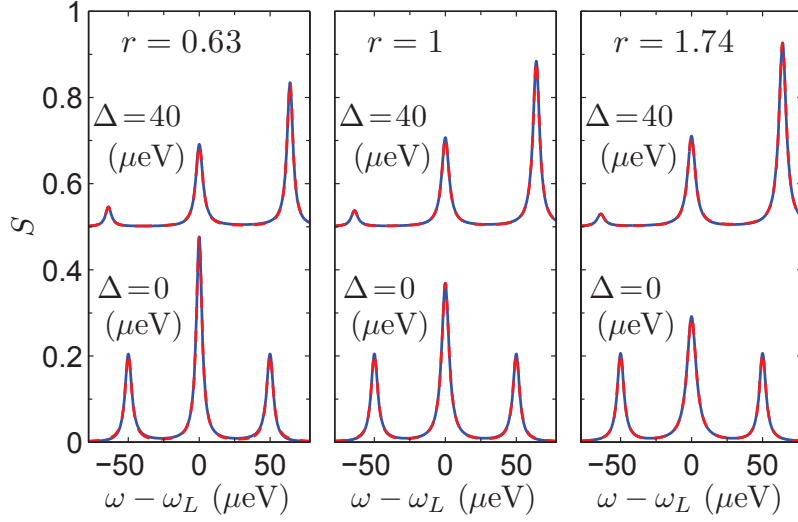
These equations are used with Eq. (10) to obtain S . We stress that the resulting spectrum is *exact* within the stated model assumptions. The full-width at half-maximum (FWHM) of spectral resonances can be obtained from Eq. (10) though these are complicated to write down analytically. However, as we have verified, one can simply fit the analytical spectrum to a sum of Lorentzian line shapes (see discussion of Fig. 4) and extract the broadening parameters.

4.4. Off-Resonant Mollow Triplet: Regimes of Spectral Sideband Broadening and Narrowing

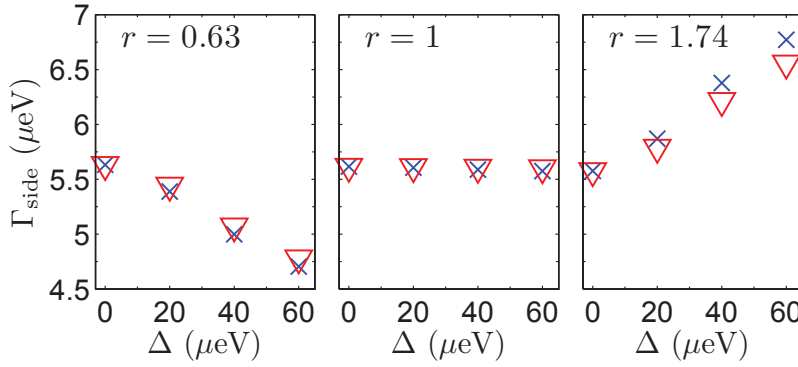
From the analytical spectra above, we can discern when the Mollow triplets will become asymmetric and whether the detuning dependence will exhibit broadening or narrowing of the three resonances. We define r as the following ratio:

$$r = \frac{\gamma_{\text{pol}} + 0.5 \gamma_{\text{cd}}}{\gamma_{\text{pop}}} = \frac{1}{2} \left[1 + \frac{\gamma' + \gamma_{\text{cd}}}{\gamma + \gamma_{\text{ph}}} \right], \quad (13)$$

where $\gamma_{\text{ph}} = \Gamma_{\text{ph}}^{\sigma^+} + \Gamma_{\text{ph}}^{\sigma^-}$. Worth to note, for off-resonant driving and $\gamma' = 0$, a completely symmetric Mollow triplet is expected *only* if all phonon terms are neglected. Thus, phonon coupling



(a) Spectra for different r values.



(b) Corresponding sideband FWHM.

Fig. 4: (a) Analytically computed spectrum as a function of detuning for three different values of r . The solid red curve shows the analytical solution [Eq. (9)] and the blue dashed curve shows the three-Lorentzian fit. Positive and negative detunings $|\Delta|$ reveal simply a mirror image of each other. The phonon parameters are taken from Fig 2, with $\gamma_{cd} \approx 0.6 \mu\text{eV}$ and $\gamma_{ph} \approx 1.6 \mu\text{eV}$ for the chosen Rabi field. Here we adjust γ and γ' to maintain the same total low-field FWHM of $\gamma_{\text{side}}(0) = 5.6 \mu\text{eV}$: For $r = 0.63, 1, 1.74$, we use $\gamma'(\gamma)$ as $3.2(2.2), 2.5(1.5)$, and $5(1.5) \mu\text{eV}$, respectively. (b) Extracted FWHM of the lower (blue crosses) and higher energetic (red inverted triangles) sideband as a function of detuning Δ . One clearly traces a trend of either increasing or decreasing sideband line width as a function of laser detuning in dependence on of r , where $r \approx 1$ denotes the crossover.

causes an asymmetry for off-resonant driving. Under systematic increase of the excitation-detuning Δ , spectral broadening or narrowing can be achieved depending upon the value of r . In Figs. 4a and 4b we plot the Mollow triplet as a function of Δ , and extract the FWHM of the sidebands for three values of r . As can be seen, $r < 1$ (for a suitably small γ') leads to spectral sideband narrowing, whereas the effect of spectral broadening occurs for values $r > 1$.

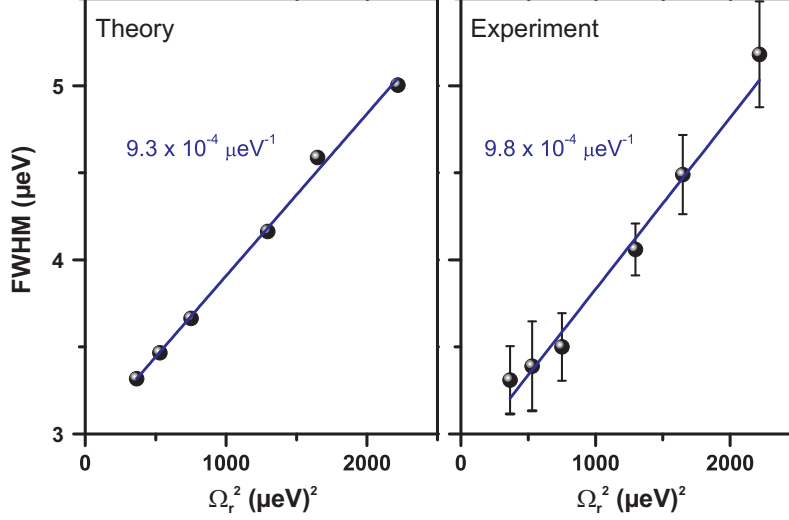


Fig. 5: Determination of the pure dephasing rate γ' . The graph shows the expected linear increase of the FWHM of the Mollow sidebands versus Ω_r^2 as extracted from a power-dependent Mollow series under strictly resonant excitation ($\Delta = 0$). A comparison between (a) the theoretical predictions (revealing a slope of $9.3 \times 10^{-4} (\mu\text{eV})^{-1}$) and (b) the experimental data (giving $9.8 \times 10^{-4} (\mu\text{eV})^{-1}$) reveals best consistency for a dephasing rate of $\gamma' = 4.08 \gamma = 3.43 \mu\text{eV}$. All other parameters are fixed according to $T = 6 \text{ K}$, $\gamma = 0.84 \mu\text{eV}$ (784 ps), $\alpha_p / (2\pi)^2 = 0.15 \text{ ps}^2$, $\gamma_{\text{cd}} = 0.13 \mu\text{eV}$, $\gamma_{\text{ph}} = 0.34 \mu\text{eV}$.

5. Comparison between Experiment and Theory

In the following, we show a detailed modeling of experimentally derived results from detuning-dependent high-resolution PL measurements with the above presented theory. The measurements are performed on a QD in a planar sample structure with negligible cavity coupling.

To reproduce the experimental results with the theoretical model we do not use fitting parameters apart from the electron-phonon coupling strength (which is obtained by fitting the observed EID), but derive all characteristic values for the calculation via independent measurements or analysis. For the cut-off frequency and electron-phonon coupling strength, we use $\omega_b = 1 \text{ meV}$ and $\alpha_p / (2\pi)^2 = 0.15 \text{ ps}^2$. The deformation potential constant is somewhat higher compared to the value used in Refs. [37, 38]. However, the value for α_p and the dimensionless Huang-Rhys parameter $S_{\text{HR}} = \alpha_p / (2\pi)^2 c_l^2 / l_{e/h}^2$ (with c_l the speed of sound and $l_{e/h}$ the and electron/hole confinement length) reported in the literature (i.e. $S_{\text{HR}} = 0.01 - 0.5$) covers a large range and there are no well-accepted numbers to date. Additionally, S_{HR} has been shown to be enhanced in zero-dimensional QDs compared to bulk material, for which different explanations are proposed, e.g., in terms of non-adiabatic effects or the influence of defects [37].

In the experiment the sample temperature has been measured as $T = 6 \text{ K}$. The QDs in the planar sample are found to have rather similar radiative lifetimes due to no Purcell-like enhancement. The radiative decay rate γ is extracted from time-correlated photon counting measurements that reveal a typical radiative lifetime of (750-850 ps), yielding $\gamma \approx (0.77 - 0.88) \mu\text{eV}$. The Rabi field $\Omega_r = 22.7 \mu\text{eV}$ is derived from the Mollow center-to-sideband splitting at zero laser-detuning $\Delta = 0$. The sum of the main phonon scattering rates $\gamma_{\text{ph}} = \Gamma_{\text{ph}}^{\sigma^+} + \Gamma_{\text{ph}}^{\sigma^-} = 0.34 \mu\text{eV}$, which is constant in the detuning range accessible in our measurements, is calculated according to Fig. 1. The cross-dephasing term has been extracted from the same graph as

$\gamma_{cd} = 0.13 \mu\text{eV}$. To carefully extract the pure dephasing rate γ' , spectra of a power-dependent Mollow triplet series of the QD under investigation at $\Delta = 0$ have been modeled with a constant γ' as the only free parameter. The extracted FWHM can be well reproduced with a pure dephasing rate of $\gamma' = 4.08 \gamma = 3.43 \mu\text{eV}$ (equivalent to a pure dephasing time of 192 ps). A direct comparison between the extracted FWHM of the experimental data and the theoretical model is shown in Fig. 5: The expected linear increase [slope: $9.3 \times 10^{-4} (\mu\text{eV})^{-1}$] in the FWHM with Ω_r^2 shows very good agreement with the experiment [slope: $9.8 \times 10^{-4} (\mu\text{eV})^{-1}$].

With all parameters at hand, the experimentally measured detuning-dependent Mollow triplet series is compared with the theoretical expectations in terms of sideband broadening and the change in the relative sideband areas $A_{\text{red/blue}} = I_{\text{red/blue}} / (I_{\text{red}} + I_{\text{blue}})$. Figure 6(a) shows a direct

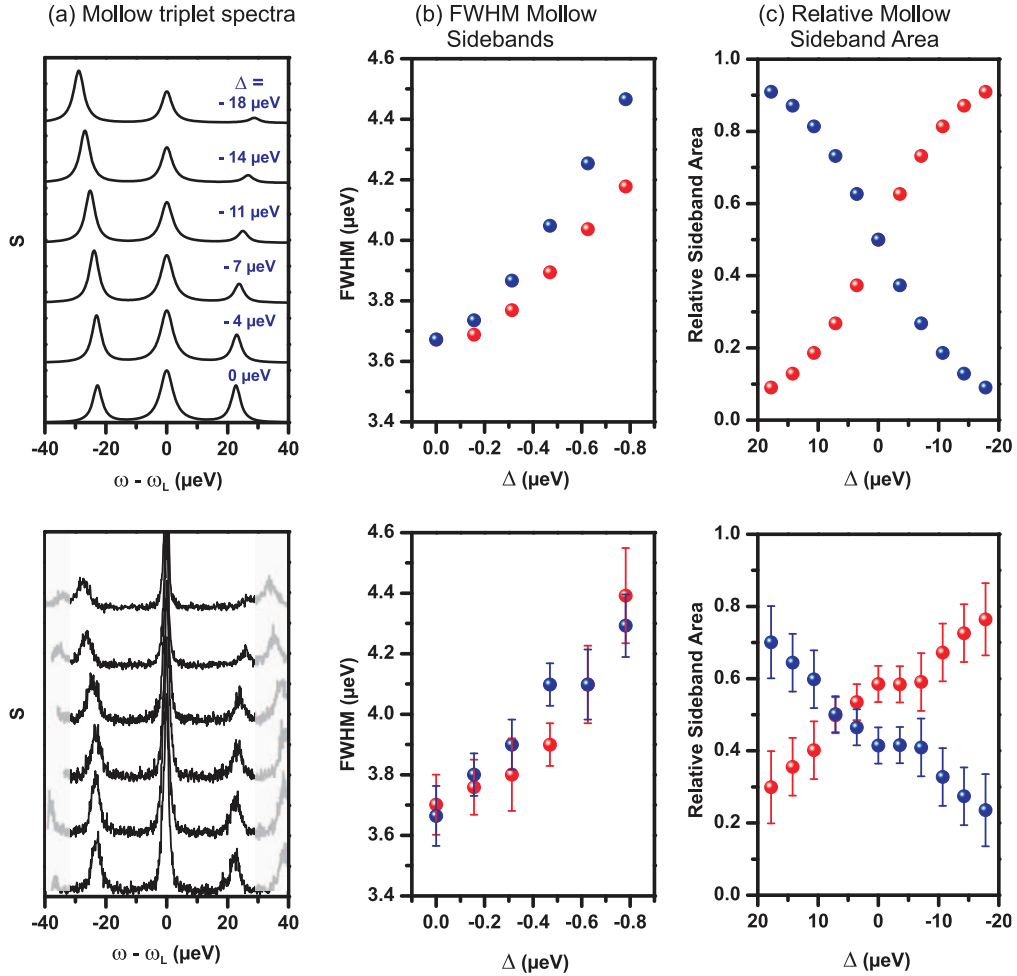


Fig. 6: Detuning-dependent Mollow triplet series at $P = 500 \mu\text{eV}$, showing theoretical predictions versus experimental results for a system with $r = 2.01$. (a) Mollow triplet spectra for increasing negative detunings, Δ , the spectra are plotted with respect to the energetic laser position set to zero. (b) FWHM of the blue and red Mollow sideband reveal distinct sideband broadening with increasing laser-detuning. (c) Change of the relative Mollow sideband area with Δ . The theoretically expected trend can be seen.

comparison of the Mollow triplet spectra for increasing negative detuning $\Delta < 0$, from which the FWHM and relative intensities are extracted. The discrepancy between the expected and measured central Mollow line intensity results from contributions of scattered laser stray-light to the true QD emission that can experimentally not be differentiated due to the equal emission frequency. For the detuning $\Delta \neq 0$ the spectral resolution of the high-resolution spectroscopy is not sufficient to distinguish between laser-excitation and QD Rayleigh line emission. The gray shaded peaks in Fig. 6(a) (lower panel) belong to a higher order interference of the *Fabry Pérot* interferometer. The extracted FWHM values are depicted in Fig. 6(b). For the system under investigation, r is calculated to be around 2.01, and therefore an increase in the sidebands' width is expected according to the theoretical model. Indeed, we observe a systematic increase with increasing negative detuning $\Delta < 0$. Additionally, the relative sideband areas $A_{red/blue}$ in dependence on Δ are plotted in Fig. 6(c). As becomes already visible from the Mollow spectra, for positive detunings the blue sideband gains intensity whereas the red sideband area decreases, and vice versa. The crossing between relative intensities is expected to occur at $\Delta = 0$. Interestingly, we observe crossings at moderate negative laser-detuning values for all different QDs under study. A detailed interpretation of the physics behind this effect has to be left for further on-going in-depth analysis (and may involve the inclusion of more excitons). All detuning dependent Mollow triplet series have revealed values of $r > 1$ and therefore a spectral broadening of the Mollow sidebands due to impurities present in the sample.

The regime of distinct sideband narrowing has also been experimentally observed by Ulrich *et al.* [18] (see Fig. 3(d) of their paper) on a QD embedded in a micropillar cavity structure, grown by molecular beam epitaxy. Even though the effect can be qualitatively understood from the theoretical model discussed above, a direct comparison to theory requires the inclusion of QED-cavity coupling into the polaron ME approach. Previous numerical studies were performed in this regime [30], but did not obtain this behaviour, suggesting that further work is required to explain the significant narrowing effects that are observed in the experiment.

6. Conclusion

In conclusion, we have presented a combined theoretical-experimental study on the impact of pure dephasing and phonon-induced scattering on the excitation detuning-dependence of Mollow triplet sidebands. Based on a polaron master equation approach, supplemented by an analytical solution for the Mollow triplet spectra, it is possible to clearly distinguish different regimes of spectral broadening or narrowing, defined by the ratio of different dephasing contributions. For the case of experimentally observed distinct sideband broadening, we have found excellent agreement with the predictions of theory. We have derived general formulas which are broadly applicable to reproduce resonance fluorescence spectra of single quantum dots without adopting a simplistic atomic model.

Acknowledgements

During the final preparation of this work we became aware of similar results obtained independently for off-resonant Mollow sideband narrowing [39]. We would like to thank Dara McCutcheon and Ahsan Nazir for bringing these to our attention and for useful discussions. S. Weiler acknowledges financial support by the Carl-Zeiss-Stiftung. The work of S. Hughes was supported by the National Sciences and Engineering Research Council of Canada.